Journal of Structural Geology 30 (2008) 948–962

Contents lists available at ScienceDirect

Journal of Structural Geology

journal homepage: www.elsevier.com/locate/jsg

Anisotropy of magnetic susceptibility and P-wave velocity in core samples from the Taiwan Chelungpu-Fault Drilling Project (TCDP)

Laurent Louis [a,*], Tzu-Mo Natalie Chen [b], Christian David [a], Philippe Robion [a], Teng-fong Wong [b], Sheng-rong Song [c]

[a] Département des Sciences de la Terre et de l'Environnement, Université de Cergy-Pontoise, CNRS UMR 7072, Bâtiment Neuville 3.1, Neuville-sur-Oise, F-95031 Cergy-Pontoise, France
[b] Department of Geosciences, State University of New York at Stony Brook, Stony Brook, NY 11794-2100, USA
[c] Department of Geosciences, National Taiwan University, 245 Choushan Road, Taipei 106, Taiwan

ARTICLE INFO

Article history:
Received 12 July 2007
Received in revised form 7 March 2008
Accepted 27 March 2008
Available online 8 April 2008

Keywords:
Anisotropy
Magnetic susceptibility
P-wave velocity
Continental drilling
Taiwan

ABSTRACT

The anisotropy of magnetic susceptibility (AMS) and anisotropy of P-wave velocity (APV) were characterized in core samples retrieved from the TCDP Hole A at depths ranging from 600m to 1400m, thus cutting across the thrust fault that ruptured during the 1999 Chi-chi earthquake. Our data show that the AMS was similar for all the samples regardless of the lithologic contrasts, with a magnetic fabric characteristic of weakly deformed sedimentary rocks that had undergone layer parallel shortening. This robust observation applies to both the siltstones and sandstones at all depths investigated. In contrast the APV data reflect fundamental differences between the elastic fabrics in the two facies. While APV of the siltstone samples is controlled by a preferred orientation of the matrix minerals, the APV of the sandstones is greatly influenced by microcrack porosity with a preferred orientation parallel to the maximum principal direction of paleostress and tectonic deformation. These AMS and APV data obtained in TCDP Hole A at locations not directly impacted by the coseismic rupture provide a first order petrofabric framework for the characterization of hydromechanical anisotropy in the Chelungpu fault system.

1. Introduction

Since the anisotropy of magnetic susceptibility (AMS) was first proposed by Graham (1966) as a tool to characterize petrofabrics and structure, the technique has been applied extensively to elucidate fabrics associated with sedimentary, metamorphic and igneous processes (e.g. Tarling and Hrouda, 1993). It has also proved effective as a petrofabric indicator of tectonic deformation and qualitative measure of finite strain (Borradaile and Henry, 1997). In particular AMS has provided important constraints on the evolution of layer parallel shortening in fold-and-thrust belts (Averbuch et al., 1992; Pares and van der Pluijm, 2002; Sans et al., 2003; Robion et al., 2007).

Unlike AMS, which derives primarily from anisotropic attributes of the solid grains in the rock matrix (such as the preferred crystallographic orientation of phyllosilicate and other tabular grains, and grain shape anisotropy of ferrimagnetic grains such as magnetite), the elastic anisotropy of a porous rock reflects the anisotropic attributes of both the solid matrix and pore space. Extensive studies have been conducted on the elastic or seismic anisotropy of different rock types (Lo et al., 1986; Hornby, 1998). These studies show that at elevated confining pressures seismic anisotropy arises primarily from lattice preferred orientation (Kern, 1993; Johnston and Christensen, 1995), and accordingly a correlation may sometimes be established between AMS and elastic anisotropy at confining pressures sufficiently high to close pre-existing microcracks in the pore space (Hrouda, 1993). However, it has also been demonstrated that at relatively low confining pressures elastic anisotropy is usually controlled by the presence of an oriented system of open microcracks, which may develop as a result of rock forming processes or tectonic deformation. Indeed Nur and Simmons (1969) demonstrated in a seminal study the correspondence among seismic anisotropy, stress-induced cracking and orientations of the applied stress field.

Recently Louis et al. (2003, 2004) introduced a methodology to characterize the anisotropy of P-wave velocity (APV) and they demonstrated for two sandstones that this velocity anisotropy can be reasonably approximated by a second rank tensor. Since the magnetic susceptibility is also described by a second rank tensor (Nye, 1957), this provides a common basis for the comparison of elastic and magnetic anisotropies. The incorporation of microstructural observations (Louis et al., 2005) furnishes complementary

* Corresponding author. Tel.: +33 1 34 25 73 48; fax: +33 1 34 25 73 50.
E-mail address: laurent.louis@u-cergy.fr (L. Louis).

0191-8141/$ – see front matter © 2008 Elsevier Ltd. All rights reserved.
doi:10.1016/j.jsg.2008.03.006

information on pore space anisotropy, grain arrangement and their influences on elastic anisotropy. This integrated methodology was adopted in the present study to investigate the AMS and APV as functions of depth and lithology in a suite of core samples from an active thrust fault system in Taiwan.

In 1999 the M_w 7.6 Chi-Chi earthquake resulted in significant casualty and damage (Shin and Teng, 2001). The main rupture of the Chi-Chi earthquake was located along the Chelungpu fault system (Fig. 1), with surface break extending over 100 km and scarps as high as 8 m in some locations. The Taiwan Chelungpu-fault Drilling Project (TCDP) is an international project to drill into this thrust fault, with the overall research goal to gain fundamental understanding of the physics of earthquakes and faulting. The vertical drilling of Hole A through the northern portion of Chelungpu fault at Takeng (near the city of Taichung) down to a depth of 2 km was accomplished in 2004. Total recovery of the mostly continuous cores from TCDP Hole A was ~97% (Song et al., 2007a).

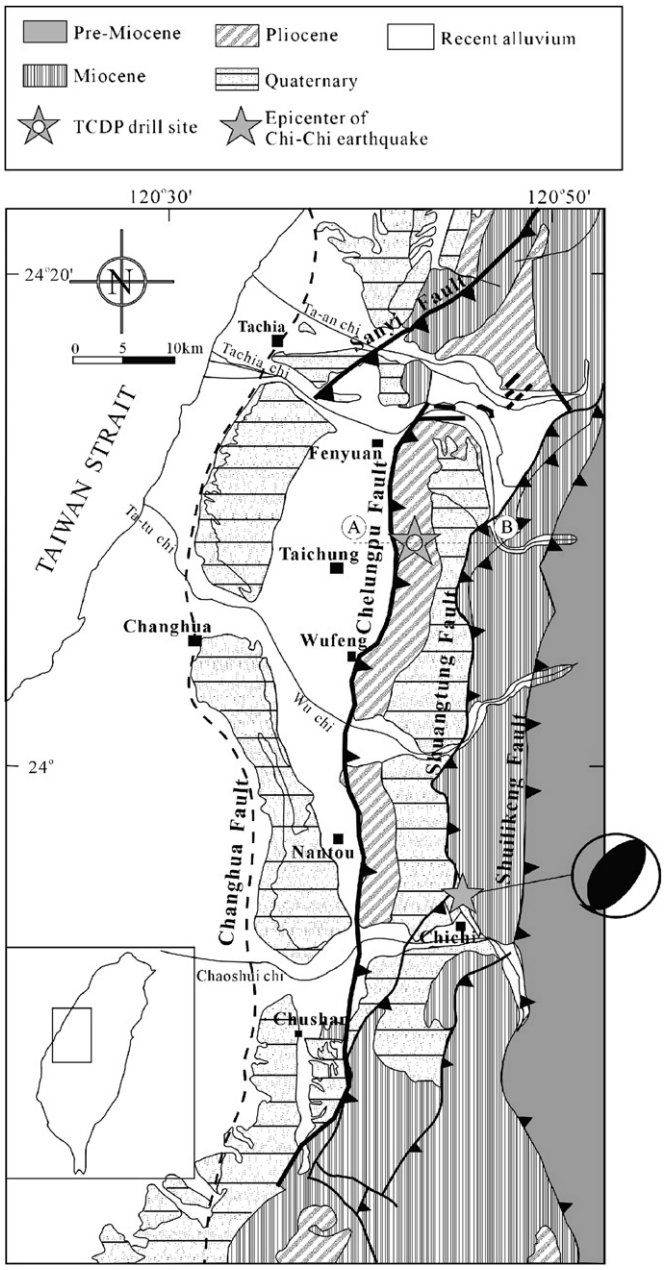

Fig. 1. Geological map of the Chelungpu-fault area in the Western Foothills of Taiwan. The 1999 surface rupture extends over ~100 km N–S. The epicenter of the Chi-Chi earthquake is located by the plain star and the TCDP drilling site by the punched star.

In this study we investigated the anisotropic behavior of a total of 15 core samples retrieved from TCDP Hole A at depths ranging from 589 m to 1412 m. To our knowledge this is the first study to consider AMS and APV of samples retrieved in the vicinity of a recently ruptured fault, thus providing a unique opportunity to address several basic questions in rock physics and earthquake mechanics. How do the AMS and APV vary as functions of depth and porosity? To what extent are these anisotropic properties related to the petrofabrics induced by tectonic deformation and stress field? Our samples can be categorized lithologically as sandstone or siltstone. Are there systematic differences between the AMS and APV of siltstone and those of sandstone? What are their implications on anisotropy of other physical properties such as permeability and static elastic moduli?

2. Sampling and method

As indicated in Fig. 2a and b, at least three stratigraphic sequences oriented N15–30E could be identified from the TCDP core samples: the Cholan formation (late Pliocene to early Pleistocene) at the top kilometer or so, Chinshui shale formation (Pliocene) at depth of 1027–1268 m, Kueichulin formation (late Miocene to Pliocene) down to 1712 m, and the Cholan formation again with subhorizontal bedding at depths below 1712 m (Yeh et al., 2007). The Cholan formation at the top is characterized by thick sandstone layers and alternating sandstone–siltstone–mudstone layers with weak to intense bioturbations. Petrographically the sandstone is predominately made up of quartz and slate fragments, with some feldspar, sandstone quartzite fragments and clay matrix. The Chinshui formation is primarily made up of siltstone, with subsidiary thin layers of fine-grained sandstone, mudstone and alternating layers of sandstone and siltstone. The Kueichulin formation is made up of thick sandstone layers, with subsidiary thin layers of siltstone and shale. Structural and deformation features indicate the existence of four fracture zones in the Chinshui shale formation (marked as FZA in Fig. 2b), with FZA 1111 considered to be the plausible location that underwent significant slip during the Chi-Chi earthquake (Kano et al., 2006; Lin et al., 2007b; Song et al., 2007b; Wu et al., 2007).

We investigated in this study 15 core samples (each ~30 cm long) retrieved from TCDP Hole A at depths ranging from 589 m to 1412 m. Six of these are sandstone and nine are siltstone. The specific depths are compiled in Table 1 and marked in Fig. 2b. Our AMS and APV measurements follow the protocol of Louis et al. (2004): from each available core, a triplet of cylindrical plugs were drilled along three perpendicular directions (Fig. 3a,b) and measured along their diameter every 22.5°. The orientation reference that was used comprises the cores axis (Z axis), the bedding dip direction (X axis) and the bedding strike (Y axis). The directional data obtained in this study will be presented in the geographical reference assuming a constant bedding dip azimuth of N105 (Yeh et al., 2007).

2.1. Magnetic measurements

The susceptibility bridge used for AMS measurements in this study was the AGICO KLY3S, which measures directional susceptibilities on a frequency of 865 Hz (AMS) with a sensitivity of 3×10^{-8} (SI). This device measures the induced magnetization $\vec{M}$ of a specimen inside a coil which generates a low alternating field $\vec{H}$. If the magnitude of the magnetization field is on the same order as that of the Earth's magnetic field, then $\vec{M}$ and $\vec{H}$ are approximately linearly related according to $M_i = K_{ij}H_j$, where K_{ij} is a second rank symmetric tensor representing the magnetic susceptibility

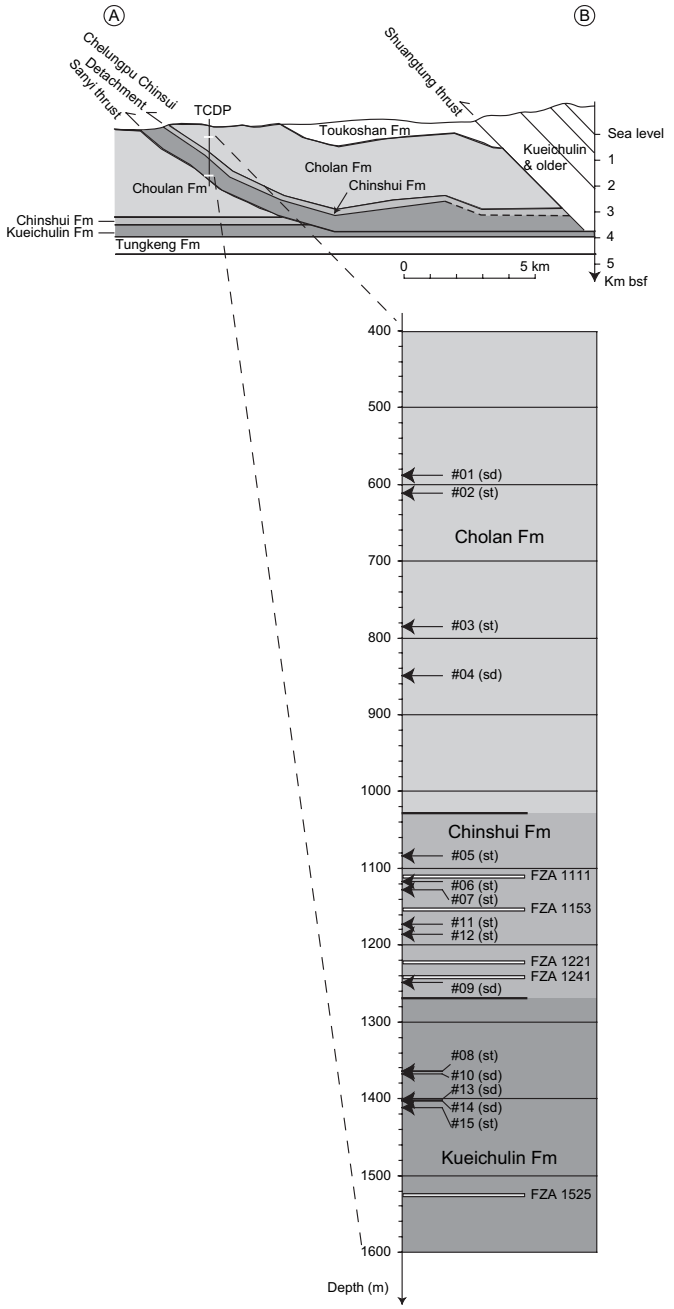

Fig. 2. (a) EW cross section passing through the drilling site (AB line in Fig. 1) (after Yue et al., 2005). (b) Sampling locations along the TCDP Hole A: a total of 15 core sections were investigated from all three formations drilled, the Chelungpu fault zone being located within the Chinshui Formation. Fault zones are as reported by Yeh et al. (2007).

(Nye, 1957; Daly, 1970). Such a relationship is valid in diamagnetic and paramagnetic materials and in magnetite bearing rocks. Pokorny et al. (2004) show that field dependence of magnetic scuceptibility may exist for some pyrrhotite, hematite and titanomagnetite rich material. This dependence concerns materials with high amount of such minerals ($K > 10^{-3}$ SI) and may affect the shape of susceptibility ellipsoid without incidence on the orientations of the principal susceptibilities.

The AMS measurements were conducted on nominally dry samples. A magnetization field was applied in a given direction and the induced magnetization in the same direction was measured with the bridge. Measurements were performed following the method described earlier. The six independent tensor elements K_{ij} were calculated from the measurements by least square inversion method. Eigenvectors and eigenvalues were then obtained by diagonalization of the susceptibility tensor.

Typically, in order to interpret AMS data two main sources of anisotropy have to be considered. For minerals with relatively low susceptibility ($<10^{-3}$ SI) such as diamagnetic (quartz, calcite), and paramagnetic (phyllosilicate) minerals, the crystallographic anisotropy dominates and shape anisotropy due to the internal self-demagnetization field is negligible. For ferromagnetic materials sensu lato (s.l.), including antiferromagnetic and ferrimagnetic minerals, this assumption may apply depending on the magnitude of the intrinsic susceptibility (Borradaile and Jackson, 2004). Magnetocrystalline anisotropy is dominant for low susceptibility ($<1 \times 10^{-1}$ SI) antiferromagnetic (hematite and goethite) and ferrimagnetic sulfide (pyrrhotite) while the shape of mineral strongly influences the magnetic anisotropy of the highly susceptible ($>1 \times 10^{-1}$ SI) ferrimagnetic minerals (magnetite and maghemite). Therefore, in sedimentary rocks the anisotropy of the susceptibility tensor K_{ij} may depend sensitively on the crystallographic orientation of the grains and on the grain shape orientation of ferrimagnetic grains such as magnetite (Tarling and Hrouda, 1993). In such rocks, the ferromagnetic s.l. fraction rarely exceeds 1% of the total volume of the rocks and one would expect the spacing among ferromagnetic grains to be so large that magnetic interaction is negligible. Despite this strong assumption, even if volume is trace (0.01%) some heterogeneity in particles distribution through the volume may cause some spurious interpretation in magnetic anisotropy directions (Borradaile and Stupavsky, 1995; Borradaile and Jackson, 2004).

2.2. Ultrasonic measurements

The ultrasonic measurements were conducted using an ultrasonic pulse generator (Panametrics 5058 PR) with an output voltage up to 900 V, P-wave transducers with a resonance frequency of 0.5 MHz, and a digital oscilloscope (HP54603B) connected to a PC for data acquisition and analysis. For each measurement the piezoelectric transmitter and receiver were located at diametrically opposite positions on the circular cross-section of a sample, and the time of flight for the ultrasonic wave to cover the diameter was measured. After the velocity profiles obtained from the three samples retrieved in each core section were corrected from slight variations in density (Louis et al., 2004), the set of 24 measurements provides travel times along 21 independent orientations for this section. Data were acquired for each sample in a nominally dry state and also after it had been saturated with distilled water. Accounting for the errors associated with picking the first arrival and measuring the sample length, we estimate the standard error for the measurements on nominally dry and saturated samples to be 0.03 km s^{-1} and 0.02 km s^{-1}, respectively (Louis et al., 2003).

Thomsen (1986) demonstrated that the P-wave anisotropy of a transversely isotropic material with relatively weak anisotropy is characterized completely by two dimensionless parameters ε and δ, which are functions of the five independent components of the elastic stiffness tensor. Specifically the P-wave speed is given by

$$V = V_o\left(1 + \delta\sin^2\theta\cos^2\theta + \varepsilon\sin^4\theta\right)$$
$$= V_o\left(1 + \delta\sin^2\theta + (\varepsilon - \delta)\sin^4\theta\right)$$

where θ is the angle between the direction of wave propagation and axis of symmetry. Recently Louis et al. (2004) showed that the P-wave anisotropy as a function of θ in most sedimentary rocks can be fitted with an error of <4% by an equation of the form $V = d\sin^2\theta + e$, and that such an approximation would imply that

Table 1
AMS and APV data obtained in the 15 sets of samples studied

AMS								
Depth (m)	Set #	Eigenvalues (.1E-06)			Average	AMS, A%	P_j	T
		K_{max}	K_{int}	K_{min}				
588.6	#01	137.98	136.91	135.68	136.86	1.68	1.02	0.07
610.7	#02	530.68	510.23	482.70	507.87	9.45	1.10	0.17
785.5	#03	222.46	219.65	216.20	219.43	2.85	1.03	0.11
850.8	#04	95.70	94.95	94.83	95.16	0.91	1.01	−0.73
1085.7	#05	409.60	401.08	389.83	400.17	4.94	1.05	0.15
1118.9	#06	501.14	487.20	470.51	486.28	6.30	1.07	0.11
1126.9	#07	413.17	401.34	393.07	402.53	4.99	1.05	−0.16
1249.2	#08	463.18	446.42	436.19	448.60	6.02	1.06	−0.23
1365	#09	219.73	214.57	210.57	214.96	4.26	1.04	−0.12
1368.4	#10	106.15	105.44	104.09	105.23	1.95	1.02	0.32
1174.5	#11	490.12	472.20	461.55	474.62	6.02	1.06	−0.24
1187	#12	572.37	554.67	535.44	554.16	6.66	1.07	0.06
1394	#13	147.76	146.70	145.29	146.58	1.69	1.02	0.15
1394.25	#14	71.93	70.95	70.65	71.18	1.80	1.02	−0.54
1411.7	#15	209.63	206.45	203.09	206.39	3.17	1.03	0.03

APV Dry									
Depth (m)	Set #	Eigenvalues (km s^{-1})			Average	APV, A%	P_j	T	Density
		V_{max}	V_{int}	V_{min}					
588.6	#01	1.83	1.49	1.28	1.53	35.25	1.42	−0.17	2.07
785.5	#03	3.14	2.96	2.78	2.96	12.13	1.13	0.03	2.48
850.8	#04	1.92	1.56	1.41	1.63	31.66	1.38	−0.35	2.10
1085.7	#05	3.58	3.42	2.93	3.31	19.49	1.23	0.53	2.57
1126.9	#07	3.90	3.73	3.51	3.71	10.35	1.11	0.13	2.59
1249.2	#08	4.04	3.71	3.44	3.73	16.06	1.17	−0.06	2.57
1365	#09	2.18	1.89	1.82	1.96	18.38	1.21	−0.60	2.35
1368.4	#10	1.85	1.50	1.25	1.53	39.14	1.48	−0.05	2.10
1174.5	#11	4.13	3.91	3.56	3.87	14.71	1.16	0.27	2.59
1187	#12	4.16	4.09	3.51	3.92	16.60	1.21	0.81	2.58
1394	#13	2.41	2.25	1.94	2.20	21.32	1.25	0.37	2.40
1394.25	#14	2.04	1.53	1.24	1.60	49.91	1.65	−0.16	2.09
1411.7	#15	2.75	2.66	2.37	2.59	14.44	1.17	0.59	2.46

APV Sat								
Depth (m)	Set #	Eigenvalues (km/s)			Average	APV, A%	P_j	T
		V_{max}	V_{int}	V_{min}				
588.6	#01	2.75	2.54	2.47	2.59	10.77	1.12	−0.48
850.8	#04	2.78	2.56	2.52	2.62	9.95	1.11	−0.65
1249.2	#09	2.78	2.65	2.59	2.68	7.19	1.08	−0.35
1368.4	#10	2.54	2.42	2.32	2.43	9.31	1.10	−0.08
1394	#13	3.07	2.99	2.88	2.98	6.26	1.06	0.14
1394.25	#14	2.47	2.22	2.06	2.25	18.10	1.20	−0.18

dAPV								
Depth (m)	Set #	Eigenvalues (km/s)			Average	dAPV, A%	P_j	T
		d_{max}	d_{int}	d_{min}				
588.6	#01	1.20	1.04	0.94	1.06	25.20	1.12	−0.48
850.8	#04	1.12	0.99	0.88	1.00	24.14	1.11	−0.65
1249.2	#09	0.79	0.77	0.59	0.72	28.37	1.08	−0.35
1368.4	#10	1.08	0.92	0.70	0.90	42.32	1.10	−0.08
1394	#13	1.12	0.86	0.73	0.90	42.59	1.06	0.14
1394.25	#14	0.85	0.70	0.41	0.65	68.40	1.20	−0.18

Shaded cells correspond to sandstone samples. While AMS measurements were performed on all samples, P-wave velocity could not be measured in sets #02 and #06 due to macroscopic fractures. Velocity data in samples saturated with water (APV Sat) were acquired in sandstone only. dAPV provides the result of the inversion for a data set consisting of the difference between water saturated and dry velocity data.

the velocity can be described by a symmetric, second rank tensor V_{ij} so that the P-wave speed for propagation along the direction n_i is given by $V_{ij}n_in_j$ (Nye, 1957). Since Thomsen's analysis (Thomsen, 1986) has been generalized by Tsvankin (1997) from a transverse isotropic to an orthorhombic material, Louis et al. (2004) concluded that the P-wave anisotropy in a weakly anisotropic rock can generally be approximated by such a symmetric, second rank tensor. Accordingly, they proposed a methodology whereby the laboratory data of P-wave velocity in multiple directions are fitted to the equation $V = V_{ij}n_in_j$ for the representation quadric, with the directions and magnitudes of the three principal axes corresponding to the eigenvectors and eigenvalues of this symmetric tensor.

The six independent tensor elements V_{ij} are calculated from the 21 measurement directions by least square inversion method. Eigenvalues and eigenvectors are then obtained by diagonalization of the velocity tensor. Fig. 4a shows typical APV data for a triplet of TCDP sandstone samples cored in the *X*, *Y* and *Z* directions and their tensor approximations for the nominally dry and saturated cases. One can notice the strong effect of water saturation on the mean P-wave velocity, as on its anisotropy. We also include in Fig. 4b the

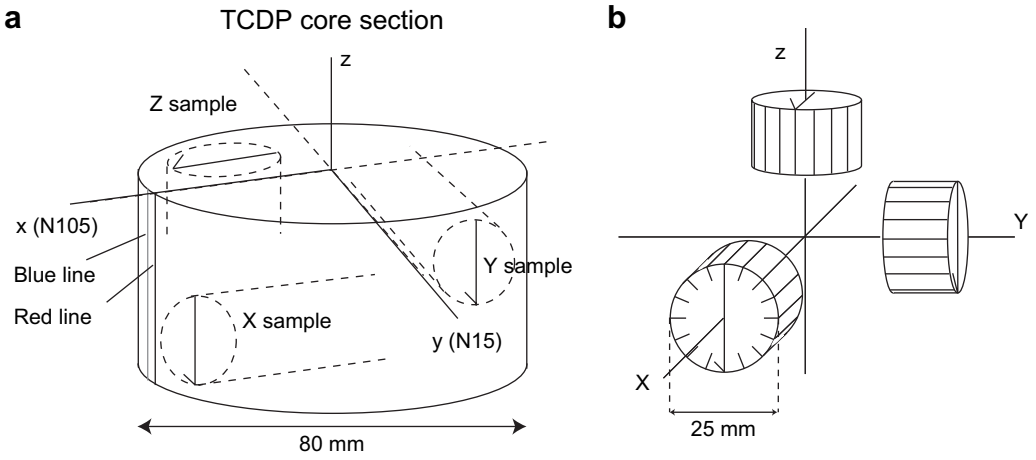

Fig. 3. (a) Sub-core sampling pattern. Three 25 mm diameter cylindrical plugs are sampled from the TCDP core section along the three reference axes. (b) Measurement protocol introduced by Louis et al. (2004): physical properties are measured parallel to the sample diameter every 22.5° (8 measures per sample). The resulting data set describes in 3D the property of the whole core section.

APV data for two sets of TCDP siltstone samples, which usually show more scatter than the sandstones.

2.3. Microstructural observation

We prepared a total of 14 petrographic thin sections of selected TCDP core samples. In particular, quantitative characterization of microcrack density and anisotropy were performed on thin sections of three sandstone samples retrieved from depths of 850.8 m, 1365 m and 1394.25 m. For each of these cores three thin sections in mutually perpendicular orientations were prepared. On each thin section 20 images at random locations were acquired under reflection at a magnification of 50×, covering a total area of 83.5 mm^2. Typically the sandstones samples are permeated with intragranular cracks. To characterize the statistical orientation of these microcracks on the digital images, we traced them and analyzed the binarized traces using ImageJ software (NIH freeware). We also performed stereological analysis on the traces. The linear intercept density is a stereological parameter defined as the number of intersections between a test array of parallel lines and a population of objects (corresponding to microcracks in this study), normalized by the total length of the test array (Underwood,

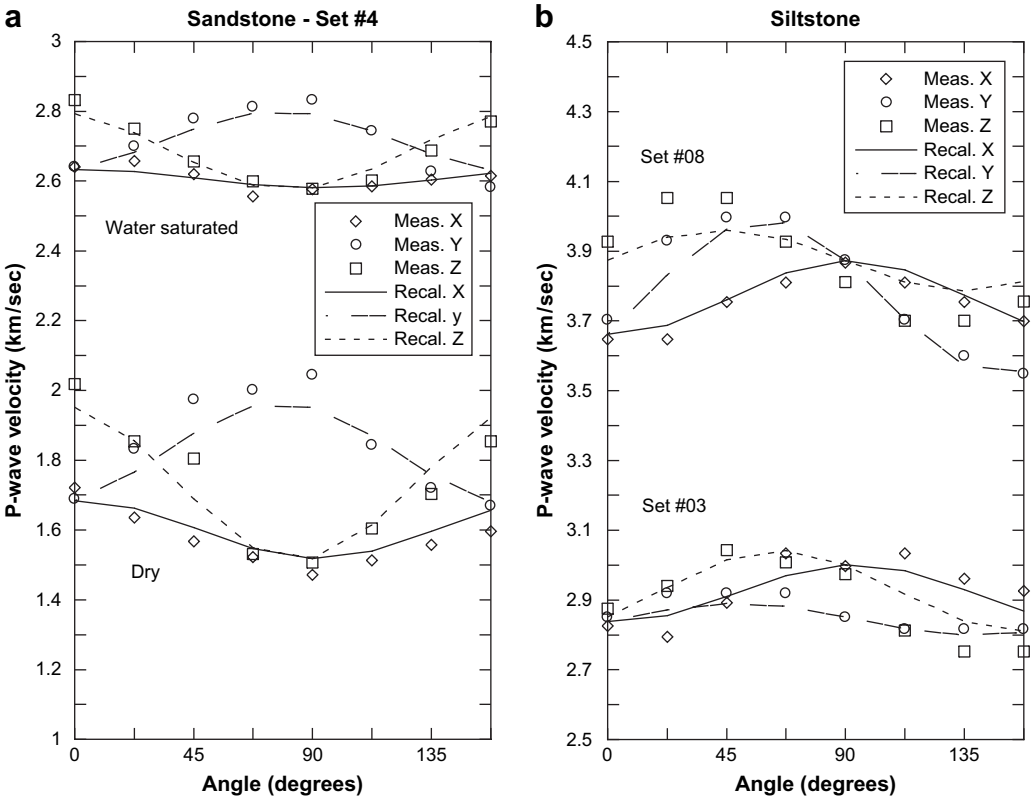

Fig. 4. (a) Typical APV data for a triplet of dry and water saturated TCDP sandstone samples cored in the *X*, *Y* and *Z* directions (Set #04, depth 850.8 m). Symbols are measurements and curves are values recalculated from the best fitting 2nd rank tensor. (b) APV data for two sets of nominally dry siltstone samples sets #03 and #08 (depths 785.5 m and 1249.2 m, respectively).

1970). To characterize the anisotropy of the linear intercept density, stereological measurements were conducted using arrays in different orientations (see Wu et al., 2000 for method). In this study a program was written with Scilab (Inria freeware) to automatically count the number of crack intercepts with 180 test arrays at angles varying from 0 to 180° with respect to the original images.

3. Magnetic susceptibility and P-wave velocity data

3.1. Bulk analysis

We will denote the eigenvalues of the magnetic susceptibility tensor by K_{max}, K_{int} and K_{min}, with $K_{max} \geq K_{int} \geq K_{min}$. Similarly the eigenvalues of the symmetric matrix fitting best the P-wave velocities are denoted by V_{max}, V_{int} and V_{min}, with $V_{max} \geq V_{int} \geq V_{min}$. These values are compiled in Table 1, which also includes the dry density. The average porosity (inferred from dry density assuming a solid grain density of 2600 kg m^{-3}) of the sandstones is about 20% and that of the siltstones close to 4%.

The magnetic anisotropy parameter $P = (K_{max}/K_{min})$ is plotted as a function of the mean susceptibility $K = (K_{max} + K_{int} + K_{min})/3$ for each sample in Fig. 5. Because K_{mean} is usually considered to be a proxy for rock composition, the dependence of the anisotropy P with K_{mean} can be seen as a test of the mineralogical control over magnetic anisotropy (Borradaile and Henry, 1997). A good correlation appears for both sandstone and siltstone samples. There is an overall tendency for K_{mean} in sandstone to be considerably smaller than for siltstone samples, which is likely due to their relatively high proportion of diamagnetic minerals (quartz, feldspar) with negative magnetic susceptibility (-14×10^{-6}). Mean susceptibilities for siltstone samples lie in a range close to typical values for paramagnetic minerals ($100–500 \times 10^{-6}$). XRD data obtained by Kuo and Song (2005) show that chlorite and illite represent about ~85% of the clay fraction in the formation samples. According to Rochette et al. (1992), $K_m \sim 400 \times 10^{-6}$ and $P = 1.3$ is the upper limit for the influence of the paramagnetic minerals. We draw in Fig. 5 the lines that correspond to the mean upper limits of P and K_m for paramagnetic rocks and minerals based on Rochette et al., (1992) and Martin-Hernandez and Hirt (2003). Above this limit we consider that ferromagnetic s.l. control the whole magnetic susceptibility, below both paramagnetic and ferromagnetic may contribute to the signal. In our case, even though the mean susceptibility lies in the higher part of this transition zone, the measured anisotropy remains very low and it is likely that the magnetic signal is mostly carried by the paramagnetic fraction. This information is of prime interest if one wants to associate directional magnetic susceptibility data to a preferential orientation of phyllosilicate minerals.

The mean velocity $V = (V_{max} + V_{int} + V_{min})/3$ and its anisotropy are plotted in Fig. 6 as a function of the bulk density of the nominally dry samples. There is an overall tendency for the mean values of P-wave velocity to be higher in the siltstone samples as compared to the sandstone, which can be explained firstly by a porosity effect, but also by the fact that a grain supported microstructure such as that of sandstones is more likely to experience intragranular cracking, which is very efficient in lowering the P-wave velocity (Budiansky and O'Connell, 1976).

We characterized the magnitude of the anisotropy of P-wave velocity (APV) by the following parameter:

$$A\% = 100^{*}\frac{V_{max} - V_{min}}{(V_{max} + V_{int} + V_{min})/3}$$

While the APV values of the siltstone samples cluster around 15%, the APV of the sandstone is more variable and reaches values as high as ~50%.

3.2. Directional data: magnetic susceptibility

All directional data is analyzed through a combination of a P_j/T plot and an equal-area lower hemispheric stereonet displaying the eigenvectors associated with AMS and APV. The P_j vs. T plot compares the corrected degree of anisotropy P_j to the shape parameter T (Jelinek, 1981). Their mathematical expressions are as follows:

$$P_j = \exp\sqrt{2\left[\left(\ln\frac{K_1}{K_m}\right)^2 + \left(\ln\frac{K_2}{K_m}\right)^2 + \left(\ln\frac{K_3}{K_m}\right)^2\right]}$$

$$T = \frac{\ln(K_2/K_3) - \ln(K_1/K_2)}{\ln(K_2/K_3) + \ln(K_1/K_2)}$$

Where K_1, K_2, K_3 and K_m are the maximum, intermediate, minimum and average principal values. Typically, P_j is a measure of the

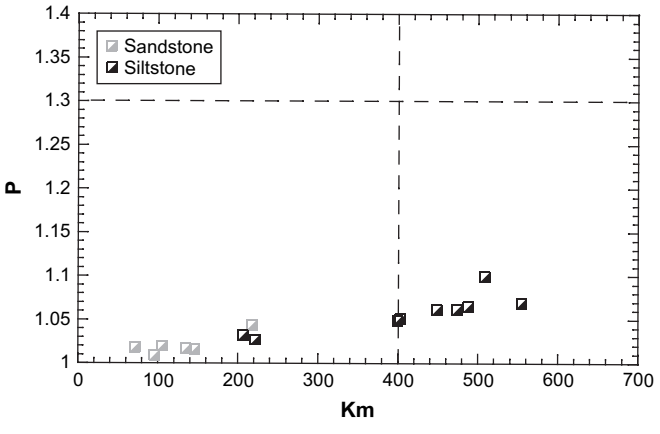

Fig. 5. Magnetic anisotropy parameter $P = (K_{max}/K_{min})$ as a function of the mean susceptibility $K = (K_{max} + K_{int} + K_{min})/3$ for all samples. The crossed dotted lines represent the limit above which paramagnetic minerals are considered not to be contributing to the magnetic susceptibility signal ($K_m > 400$; $P > 1.3$) (Rochette et al., 1992). The low anisotropy coefficient allows us to consider the signal as being partly controlled by diamagnetic and paramagnetic mineral fractions.

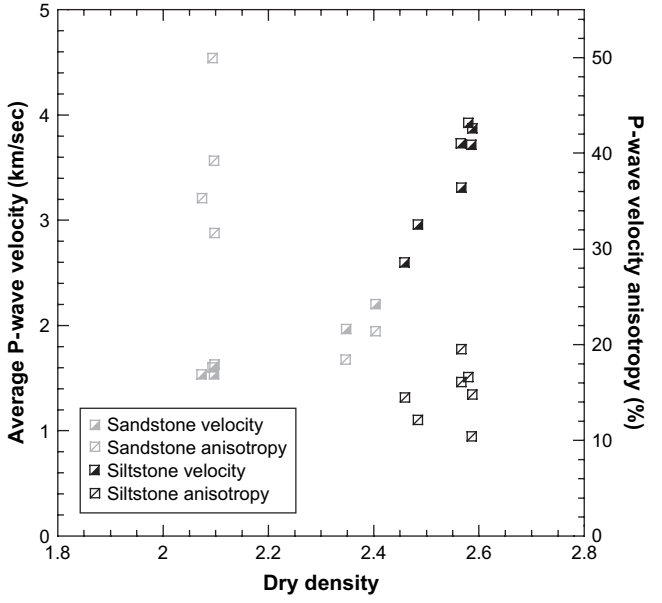

Fig. 6. Average values of P-wave velocity as a function of dry sample density (filled symbols) and corresponding P-wave velocity anisotropy (open symbols). Lighter sandstone shows lower P-wave velocity and much higher velocity anisotropy than denser siltstone.

sphericity of the ellipsoid, and T is the shape parameter that is negative ($-1 < T < 0$) when the fabric is linear and positive ($0 < T < 1$) when the fabric is planar (Jelinek, 1981).

All our AMS data are compiled in Fig. 7a and b. For comparison we also plot in Fig. 7b the bedding plane and pole in the TCDP cores, the orientation of the dip line being (N105–30E) with a variability of the dip angle with depth of about ±10° (Yeh et al., 2004).The P_j vs. T plot of Fig. 7a shows a tendency of the siltstone samples to bear higher magnetic susceptibility anisotropy than sandstone samples. The shape parameter of a majority of the samples indicates close to zero T values (triaxial magnetic fabric), except for two sandstone samples which also show very small anisotropy. It should be noted here that T is basically a difference between the lineation parameter $L = K_1/K_2$ and the foliation parameter $F = K_2/K_3$ that are used in Flinn diagrams. Regardless of the total anisotropy, should either one of these parameters be equal to one (two principal values equal to each other), T would take a value of −1 or 1, indicating pure lineation or pure foliation. It is clear from this observation that for close to spherical fabric, extreme T values should not be regarded as meaningful information (Borradaile and Jackson, 2004). The lineation of a relatively undeformed sedimentary rock is usually quite small relative to the foliation (Kligfield et al., 1981). This is due to the nature of sedimentary deposition and subsequent compaction that tends to reorient non spherical particles parallel to the bedding plane. In all samples in Fig. 7a, T values show clearly that fabrics are rather triaxial, i.e. with three distinct principal values. In Fig. 7b, the AMS principal directions stereoplot provides a robust result in that the AMS eigenvectors in the sandstone and siltstone samples fall into three distinct clusters regardless of the facies. The principal directions associated with K_{min} in all 15 samples cluster in the vicinity of the pole of the bedding plane while K_{max} is roughly parallel to the strike of the bedding at right angle to the main tectonic shortening direction. K_{int} falls into a cluster aligned near the bedding plane, subparallel to the shortening direction. Such a magnetic fabric can be considered as characteristic of weakly deformed rocks that have been subjected to "layer parallel shortening" (Robion et al., 2007), provided that the orientations of K_{max} and K_{int} are consistent with the structural directions.

3.3. Directional data: P-wave velocity

Unlike AMS data, P-wave velocity data are very sensitive to the lithology. The result of our measurements in nominally dry sandstone and siltstone are presented in Fig. 8a–c. Fig. 8a is the P_j vs. T diagram. As compared with AMS data, P-wave velocity values are much more anisotropic. Siltstone and sandstone samples differ quite clearly from one another. The siltstones have a rather stable anisotropy and positive T values indicating planar microstructural fabric. The sandstone samples tend to have more linear fabrics and very high anisotropy (up to 1.7). The fabric contrast between the two lithologies is also underscored by fundamental differences in the orientation of the eigenvectors relative to the pole of the bedding. In sandstone (Fig. 8b), V_{min} is measured parallel to the bedding strike, while it is close to the pole to bedding in siltstone (Fig. 8c), in a position consistent with the AMS results. Also, V_{max} and V_{int} are somewhat dispersed (close values) in a plane close to the bedding in the siltstone samples, while in the sandstone, V_{max} clusters clearly at right angle to the bedding strike in a subhorizontal position.

The elastic fabric we observe in the TCDP siltstone samples is qualitatively similar to previous data on relatively undeformed sedimentary rocks and metamorphic rocks. Hrouda et al. (1993) reported strong correlation between magnetic and elastic anisotropies (measured at elevated pressures) attributed to the preferred orientation of the phyllosilicate minerals. They also observed that the APV in their samples were enhanced by the existence of open microcracks aligned parallel to the bedding plane. Similar elastic fabric (with the V_{min} axis subparallel to the bedding pole) in shale was also reported by Johnston and Christensen (1995), who attributed the seismic anisotropy to the preferred orientation of illite and microcracks subparallel to bedding.

In the sandstone samples, preferred orientation of clay minerals (or microcracks) along the bedding plane cannot explain solely the fabric in Fig. 8b. This fabric might rather be caused by the presence of a parallel set of microcracks with normal direction oriented along the bedding strike.

To gain further insight into the origin of the APV in the sandstones, we performed different additional measurements that are all sensitive to the pore space. First we saturated the samples with distilled water and repeated the ultrasonic measurements. The resulting fabrics (Fig. 9a) are qualitatively similar to those of the dry sandstones, in that the eigenvectors are located in three clusters at almost the same locations. However, the magnitudes of the velocities are higher while values of the anisotropy parameter $A\%$ are smaller in the saturated samples (Table 1, also Fig. 4a), which can be attributed to an unevenly distributed change in the pore space

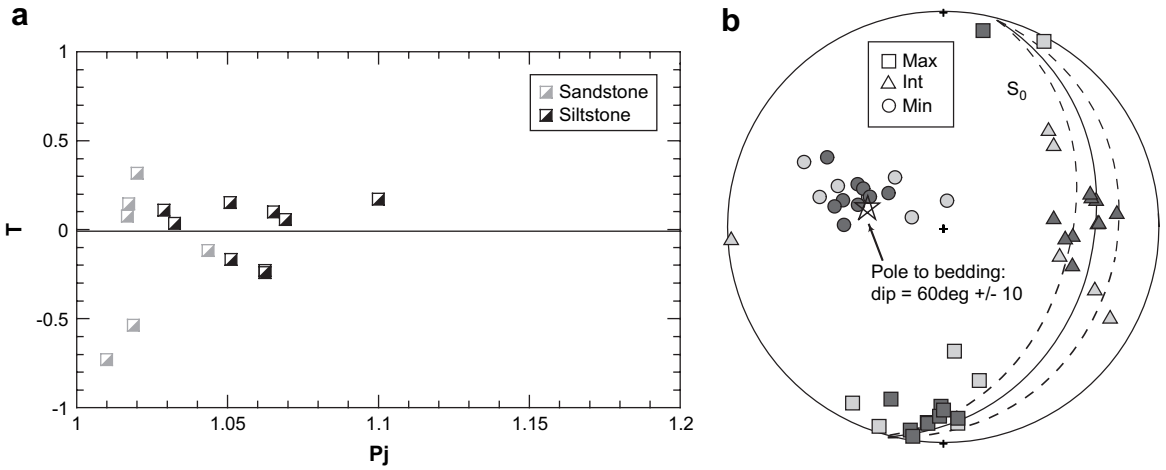

Fig. 7. (a) T vs. P_j plot of the magnetic susceptibility in sandstone and siltstone. Both lithologies show fabrics that have probably evolved under deformation from initially planar sedimentary fabrics to triaxial fabrics ($K_1/K_2 \sim K_2/K_3$). (b) Equal-area lower hemisphere projection of the principal susceptibility axes for the 15 sets of samples measured (light grey symbols: sandstone; dark grey symbols: siltstone). The whole data set tends to cluster in the same areas with a minimum susceptibility axis perpendicular to the bedding and a maximum susceptibility axis parallel to the bedding strike.

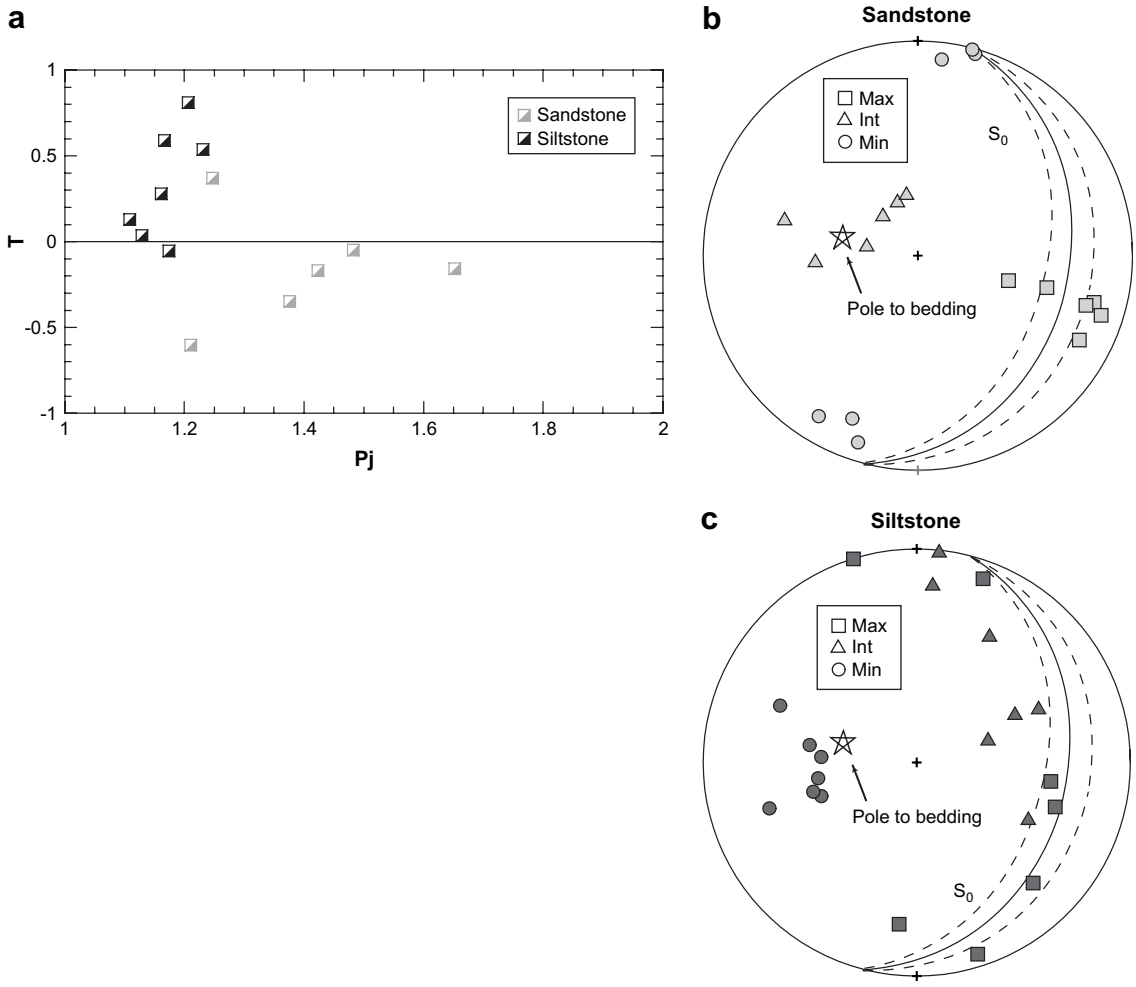

Fig. 8. (a) T vs. P_j plot of the P-wave velocity in sandstone and siltstone. Siltstone samples show rather planar fabrics (sedimentary related) while P-wave velocity fabrics in sandstone are more linear, confirming distinct microstructural characteristics. (b) APV data for sandstone samples. The minimum velocity axis is aligned with the bedding strike and maximum velocity value lies close to the bedding dip line. (c) APV data for siltstone samples. The minimum velocity axis clusters near the bedding pole and maximum and intermediate velocity axes scatter close to the bedding plane.

contribution to the elastic properties after water saturation. In a previous study, Louis et al. (2003) proposed the use of the P-wave velocity contrast between nominally dry and water saturated samples to characterize the effect of the pore space anisotropy. Fig. 9b shows the result for the inversion of such a data set. Minimum velocity differences are observed close to the bedding dip azimuth, while maximum velocity differences are found subparallel to the bedding strike.

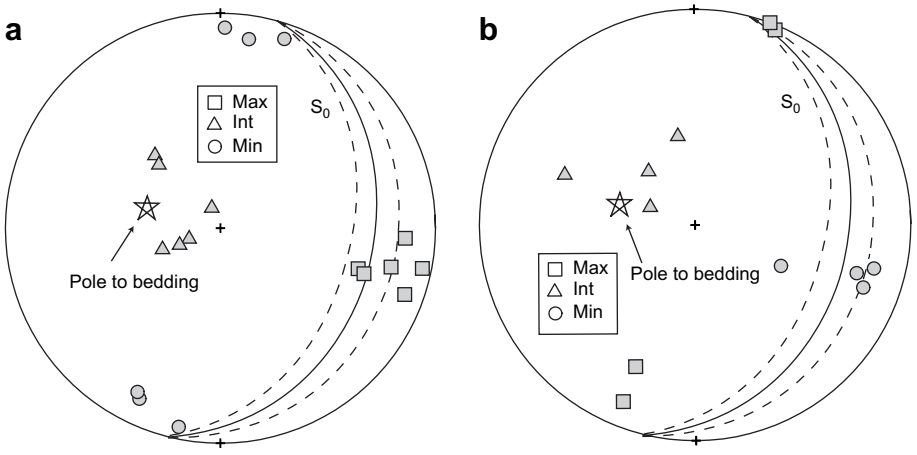

Fig. 9. (a) APV data for water saturated sandstone. The location of the principal axes is similar to the pattern observed in dry samples. (b) P-wave velocity difference between saturated and dry sandstone samples. Triaxial fabric suggests a combination of two planar anisotropy sources within the pore space.

We also performed magnetic susceptibility measurements on a sandstone sample saturated with ferrofluid and electrical conductivity measurements along directions N15 (bedding strike) and N105 (bedding dip azimuth). The ferrofluid saturation experiment is a method that involves filling the pore space of a rock sample with a suspension of ultrafine magnetic particles (Pfleiderer and Halls, 1993; Benson et al., 2005; Louis et al., 2005). Given the very high susceptibility of the suspension, the magnetic signal measured after saturation of an anisotropic void space is expected to reflect this anisotropy. The result for this measurement is shown in Fig. 10a. In a way very similar to what has been observed for P-wave velocity, the minimum magnetic susceptibility of the sample saturated with ferrofluid is oriented along ~N201 at small angle to the horizontal, therefore subparallel to the bedding strike, and the maximum susceptibility is measured perpendicular to the bedding strike at the exact same location where maximum velocities have been observed in Fig. 8b.

If a crack network with a preferential orientation is present in the sandstone samples, then the electrical conductivity should reflect the anisotropy due to a significantly lower resistance to transport along the crack planes. Electrical measurements were performed with a Radiometer CD210 conductimeter. The conductivities were measured along the axis of the *X* and *Y* cores of sample sets #1 and #10 (directions given in Fig. 10a). The samples were successively saturated with three brines (NaCl solutions) with increasing conductivities (~0.1 S m^{-1}, ~0.5 S m^{-1} and ~1.4 S m^{-1}). We followed the procedure given by David et al. (1993) and estimated the formation factor *F* and surface conductivity σ_s using the relation:

$$\sigma_r = \frac{1}{F}\sigma_w + \sigma_s$$

where σ_r is the rock conductivity and σ_w the brine conductivity. As the electrical conductivity of the solid phase can be considered virtually naught when compared to brine conductivity, electrical conductivity measurements provide information on the geometry of the pore space. The results for the two sample sets are given in Fig. 10b. The values of the formation factor and surface conductivity derived from each linear trend are given in Table 2. For both sets, the formation factor which is basically the inverse of the slope of the linear trends is systematically lower in the *X* sample, i.e. along N105, while according to the bedding orientation one would expect the conductivity to be higher parallel to the bedding surface. This observation suggests that a feature that facilitates transports in a direction oblique to the bedding is present in the microstructure, and this is again consistent with the presence of a network of parallel cracks perpendicular to the bedding strike (i.e. along N105). It should be noted that the slight shift in the measured conductivities that is observed between the two sets can be attributed to a difference in porosity of about 1% between the sets (see Table 2).

Overall, these observations reinforce the idea that sandstone bears a strongly anisotropic pore space. If indeed APV of the sandstones is controlled by a set of parallel cracks in contrast with siltstones where phyllosilicates preferentially aligned along the bedding plane are assumed, then the two lithologies must exhibit fundamentally different microstructures.

4. Microcrack density and anisotropy

Fig. 11 compares the rock microstructure for the two lithologies under the microscope using the same magnification. The sandstone sample #01 (Table 1) shows a grain-supported microstructure with relatively large grain size and appreciable intragranular cracking (Fig. 11a), while the siltstone sample #08 is composed of a relatively compact clay-rich matrix completed by relatively small quartz grains (Fig. 11b). As far as the siltstone samples are concerned, the elastic fabric obtained from the P-wave velocity measurements is consistent with the AMS results and also with the assumption that the whole rock microstructure and properties were characterized by a preferential alignment of clay minerals, as documented in previous studies (e.g. Johnston and Christensen, 1995). In the case of the sandstone, the microcracks can significantly influence both the magnitude and anisotropy of the sonic velocities. To characterize this microstructural influence, we used two complementary methods to evaluate quantitatively the microcrack density and anisotropy in nine thin sections from three sandstone cores.

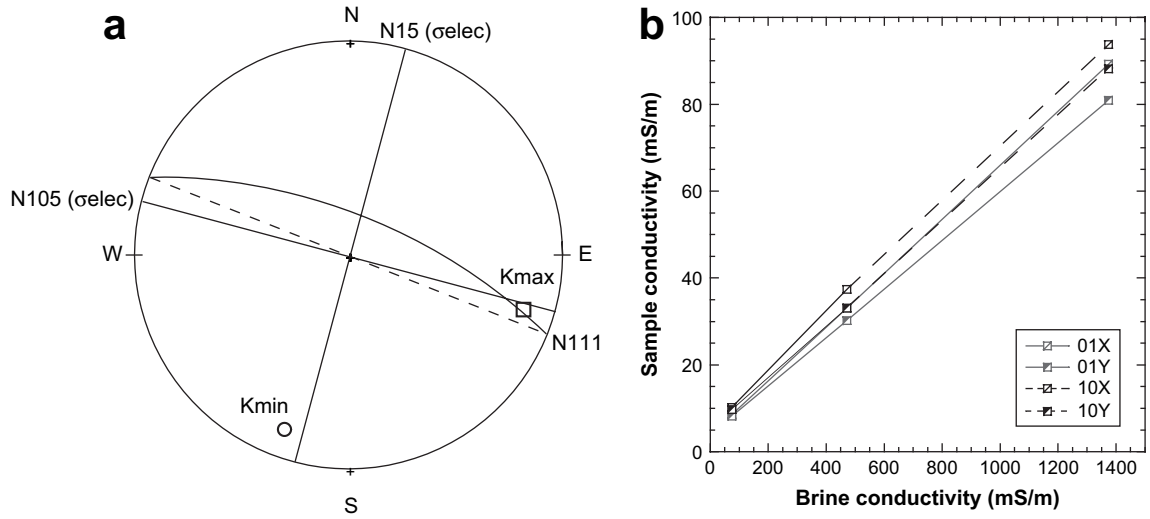

Fig. 10. (a) AMS data obtained on sandstone sample saturated with ferrofluid. The minimum magnetic susceptibility lies close to the bedding strike (also maximum velocity difference in Fig. 9b). The traced plane contour materializes the high dip AMS foliation perpendicular to K_{min}. Straight plain lines represent the directions along which electrical conductivity was measured. (b) Results of the electrical conductivity measurements. The sample conductivity is plotted as a function of the brine conductivity and the inverse of the slope of the linear trends provides values for the formation factor *F*. Therefore the higher the slope, the lower the formation factor. Grey lines and dots correspond to data obtained in sample set #01 and black dots and dotted lines to data obtained in sample set #10. In every set, the formation factor is higher along the *Y* direction (N15) as compared to the *X* direction (N105), therefore transport appears facilitated along direction N105.

Table 2
Electrical conductivity data obtained in *X* and *Y* samples from sets #1 and #10

Sample	Porosity (%)	Formation factor	Surface conductivity (mS m^{-1})
#01*X*	18.2	16.1	3.84
#01*Y*	18.4	17.8	3.93
#10*X*	19.3	15.6	6.13
#10*Y*	19.3	16.5	4.92

Thin sections in three mutually perpendicular orientations were prepared from each of three core samples from depths 850.8 m, 1365 m and 1394.25 m (sets #04, #09 and #14). Our convention for surface orientation and photographs obtained from set #04 are shown in Fig. 12a. On the photographs (Fig. 12b–d) one can easily notice a relatively intense intragranular cracking on surfaces (*X*) (perpendicular to azimuth N105) and (*Z*) (horizontal surface) as compared to surface (*Y*) where relatively few cracks are observed.

Most of these intragranular cracks are such that they can be approximated as quasi-linear features on the thin sections. We traced these cracks, mapped them on the images as linear features, then measured the statistical distributions of the trace lengths and orientations. In each sample more than 10,000 cracks with lengths in the order of 10–100 μm were measured (Table 3). To characterize microcrack anisotropy, the crack population mapped out in each thin section was grouped into bins of 10°. The nine polar plots in Fig. 13 are the result of this statistics. We also conducted stereological measurements of the linear intercept density, which represents a reciprocal measure of the crack density (shown in the polar plots) that is out of phase by 90°. Our stereological data acquired at angle increments of 1° are shown as solid curves in Fig. 13. On a 2-dimensional image, if the microcracks are preferentially aligned along an angle θ, then the linear intercept density (as a function of orientation of the test array) will attain a maximum at the orthogonal angle $\theta + 90°$ (Underwood, 1970). The complementary nature of these two types of measurements is well illustrated in our data. As can be observed in Fig. 13b, *Y* sections which correspond to vertical surfaces cut perpendicular to N15 show fewer cracks than the other surfaces. In sections representing plane (*X*) (Fig. 13a) a maximum crack count (or minimum linear intercept) is observed near the vertical direction (from N15: 90 °, 70 °, 65 °, for 04*X*, 09*X* and 14*X*, respectively), and Fig. 13c shows that cracks traces in horizontal planes (denoted (*Z*)) are preferentially aligned with azimuth N105.

If the microcracks can be approximated as planar discontinuities, then their preferred orientations as projected on three orthogonal planes can be used to constrain the orientations in 3-dimensional space. Because the stereological measurements were acquired at relatively small angular increments, the variation of linear intercept density with orientation is relatively smooth allowing both the maximum and minimum to be readily identified in our data. The minimum in intercept density corresponds to the preferred orientation of the cracks projected on the thin section. For every set investigated, the preferred orientations identified in three mutually perpendicular sections would constrain the plane that represents a best-fit approximation to the preferentially oriented crack idealized as a planar discontinuity. The preferentially oriented planes (and their poles) of our three core samples so constrained are plotted in Fig. 13. For comparison we also plot in this figure the orientations of the velocity eigenvectors from Fig. 8b. The microcrack and P-wave anisotropies are consistent in that the crack poles are found to be subparallel to the general minimum velocity directions, while the maximum velocity vectors lie near the crack planes. Quantitative characterization of the microcrack anisotropy has provided a microstructural basis for the P-wave anisotropy observed in the TCDP sandstone core samples.

5. Summary and discussion

A key conclusion from our AMS data is that the magnetic fabrics of both sandstone and siltstone samples of TCDP are characteristic of sedimentary rocks that have been subjected to layer parallel shortening. This robust observation applies to both facies over the broad range of depths we sampled, with the principal directions associated with K_{min} clustering in the vicinity of the pole of the bedding, and the maximum susceptibility axis aligned along the bedding strike.

From extensive measurements of stress orientation indicators (such as fault slip and fold axes) in the fold-thrust belt of the Western Foothills in Taiwan, Angelier et al. (1986) concluded that the maximum compression direction of paleostress was as indicated in Fig. 14b (orientation denoted by ii). This paleostress orientation is subparallel to the overall bedding dip direction measured in TCDP core samples (Yeh et al., 2007) and close to the maximum horizontal stress S_{Hmax} deduced from borehole breakouts in TCDP holes A (Wu et al., 2007) and B (Lin et al., 2007a) (orientation iii in Fig. 14b). Our results are very consistent with these observations from both AMS and APV perspectives.

Similar AMS studies have been conducted on oceanic drilling cores retrieved from somewhat smaller depth ranges. In the Nankai Trough above the décollement Owens (1993) observed the consistent development of a magnetic fabric similar to that of our

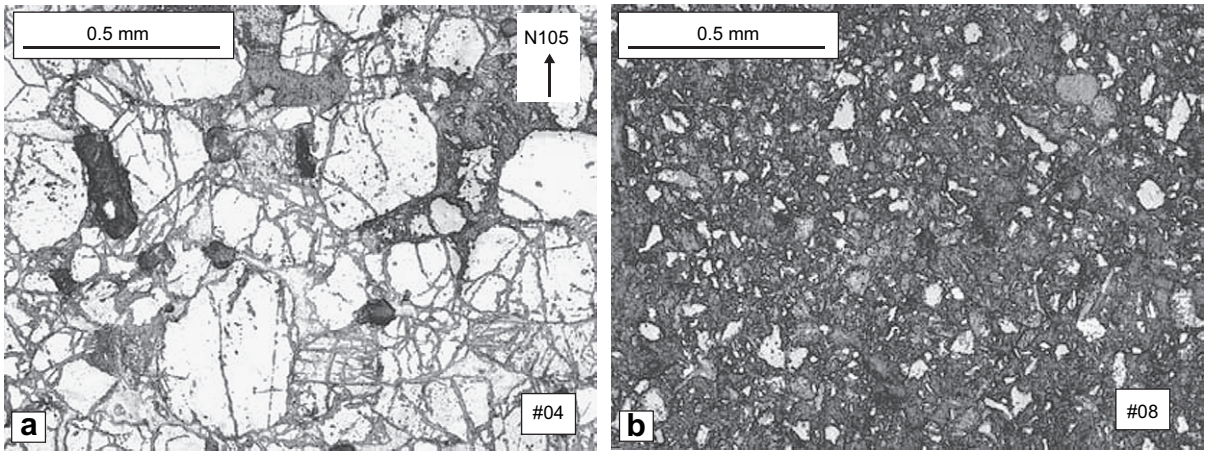

Fig. 11. Comparison between sandstone and siltstone microstructures. (a) Sandstone microstructure is grain-supported with relatively large grain size and intragranular cracking. (b) Siltstone microstructure is supported by a clay-rich matrix containing small dispersed quartz grains.

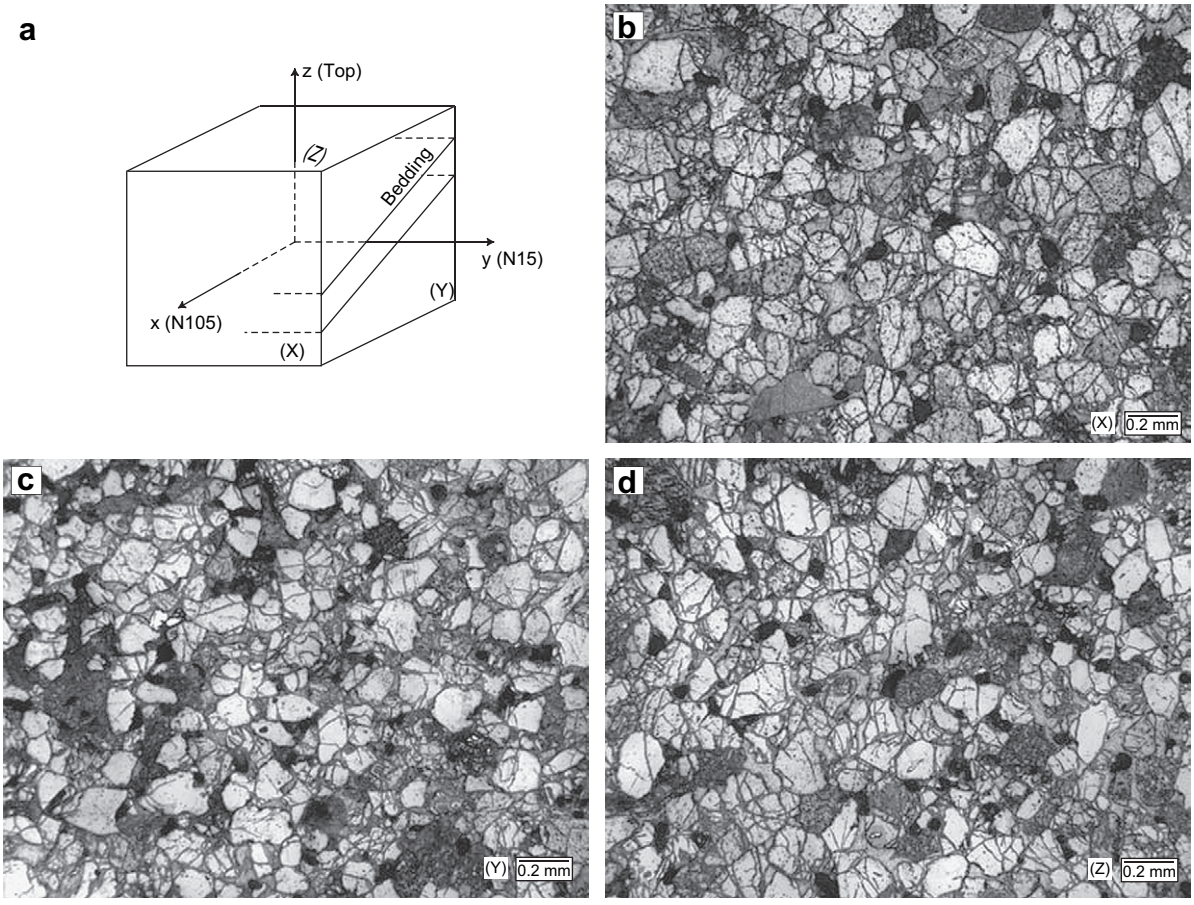

Fig. 12. (a) Schematic of the thin sections surfaces orientation. Sections were cut with respect to the core reference, i.e. the surfaces analyzed correspond to the basal planes of the plugs shown in Fig. 3. Sections were named after their normal axis (for instance the surface perpendicular to direction x was called (*X*)). (b–d) Photographs of thin sections cut along planes (*X*), (*Y*) and (*Z*) in set #04. One can notice intense intragranular cracking on (*X*) section (perpendicular to azimuth N105) and (*Z*) (horizontal section) as compared to (*Y*) section.

TCDP samples. In the Barbados accretionary prism Housen (1997) observed a more evolved AMS fabric with minimum susceptibility axis aligned along the shortening direction. In both studies core samples retrieved below the décollement zone showed AMS fabrics characteristic of sedimentary (i.e. undisturbed) fabrics, which indicates that these samples were decoupled from strain accumulation above and in the vicinity of the décollement. Such a "sedimentary" fabric was absent in our TCDP cores, possibly because the samples retrieved at depths below the Chelungpu thrust had also been subjected to layer parallel shortening since they were located within the hanging wall of the Sanyi thrust below.

Our study demonstrates the usefulness of integrating AMS and APV measurements to gain additional insights into petrofabric investigations. Our APV measurements show that the elastic fabric is sensitive to lithology, and in conjunction with our AMS measurements on samples saturated with ferrofluid and quantitative microstructural observations they indicate that APV in sandstones is controlled by the anisotropy of microcracks. Because of the relatively low density of microcracks in the siltstones, the preferred alignment of clay minerals in these samples can simultaneously exert dominant influences over both their APV and AMS. Hence the elastic fabrics reflect fundamentally different modes of strain accumulation in sandstone and siltstone. In response to the applied stress field, sandstone tends to deform in a brittle manner with development of stress-induced microcracking that is manifested by velocity anisotropy (Nur and Simmons, 1969). In contrast, microcracking was not as pervasive in the relatively "ductile" siltstones and accordingly their APV was primarily controlled by orientation of clay minerals. At this time, no further determination of microstructural deformation features was performed. It is possible that strain was accommodated through other mechanisms as well, such as crystal plasticity or diffusion creep. In a recent study, Isaacs et al. (2007) conducted geochemical and microstructural analyses of Chelungpu fault related rock samples retrieved both from the field and from TCDP hole A. In TCDP hole A, the authors reported by places the presence of deformed quartz grains and undeformed fossils and bioclasts away from the fault zones. No systematic features related to long term deformation other than the ones that were addressed in the present paper were evidenced, at least at the scale of their investigations.

Evaluation of the P-wave velocity anisotropy in samples from other drilling sites such as the Nankai Trough (Brückmann, 1993;

Table 3
Data from crack study in sample sets #04, #09 and #14

Set #	Sample	Total crack count	Mean length (μm)	Preferred orientation	Planar best fit (strike, dip)
#04 (850.8 m)	*X*	13857	94.9	N15/89	N101.1, 89.5S
	Y	2978	106.7	N105/55	
	Z	5535	121.1	N100/0	
#09 (1365 m)	*X*	15381	67.5	N15/81	N285.5, 84.3N
	Y	4700	93.5	N105/53	
	Z	8777	90	N103/0	
#14 (1394.25 m)	*X*	16564	74.4	N15/71	N288.3, 77.1N
	Y	10087	95.7	N105/51	
	Z	13362	94.1	N103/0	

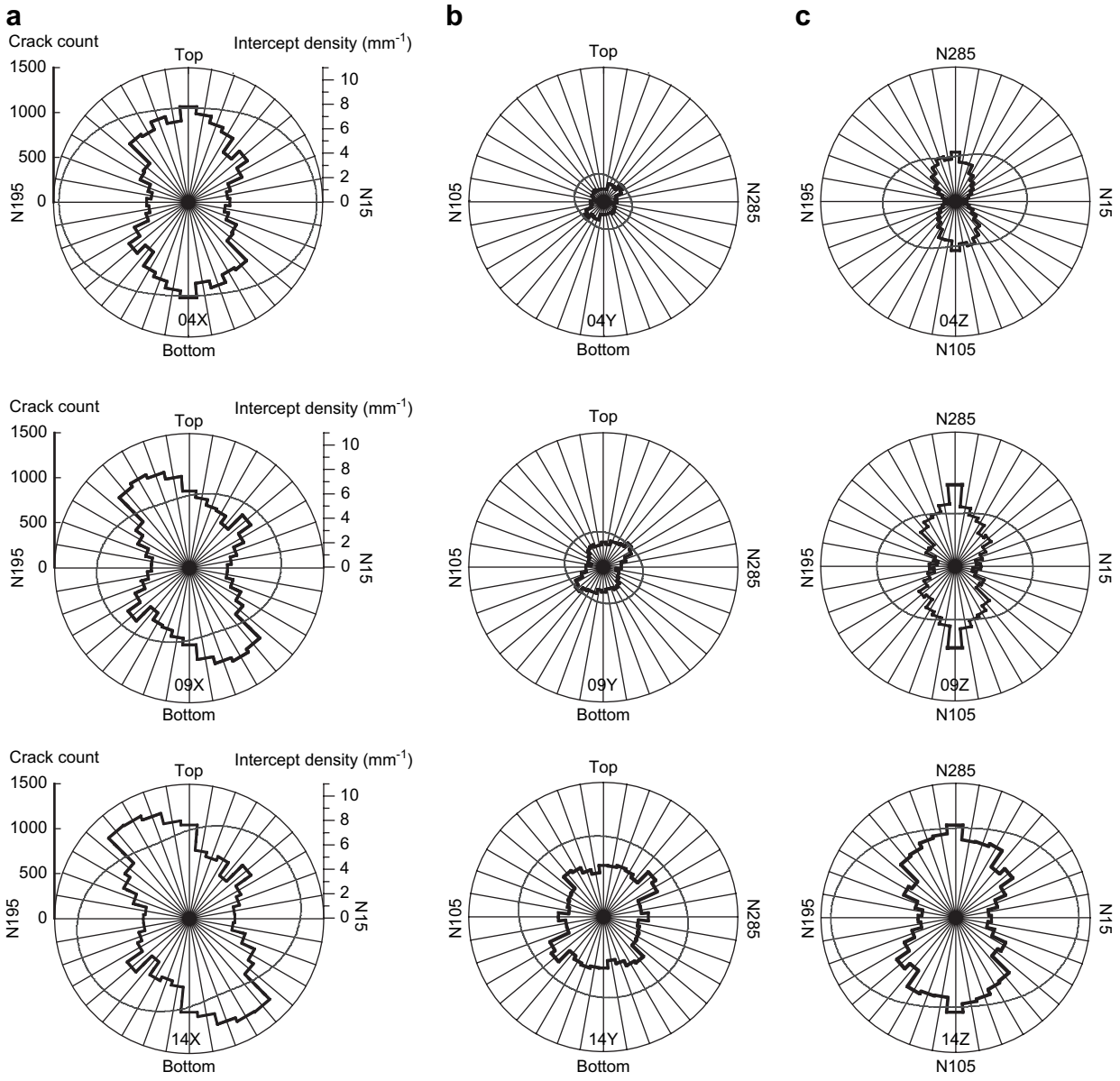

Fig. 13. Polar plots of crack orientation and crack intercept density obtained from thin sections in plug sets #04, #09 and #14. Columns (a) to (c) correspond to sections (*X*) to (*Z*). (*Y*) sections contain fewer crack traces than other sections. Maximum crack counts in sections (*X*) and (*Z*) are obtained along or close to the vertical and along azimuth N105, respectively.

Byrne et al., 1993) and the Barbados ridge accretionary complex (Brückmann et al., 1997) had led to similar conclusions that deserve comparison with our results. In the Nankai Trough (Brückmann et al., 1993), P-wave velocity maximum and minima were attributed to the presence of microcracks originating from regional tectonics (parallel to the direction of convergence) and from stress relief after sample recovery (perpendicular to the direction of convergence). In relatively homogeneous silt clay samples, Byrne et al. (1993) observed a single anisotropy in the horizontal plane with a maximum P-wave velocity measured perpendicular to the maximum compressive stress which can be related to the preferred alignment of clay minerals (also evidenced by AMS measurements).

Our P-wave velocity results in sandstone can be explained with the scheme provided in Fig. 15. A sedimentary fabric first formed during deposition and compaction. This sedimentary fabric, depending on the depositional regime, might have been made of an isotropic surface oriented parallel to the bedding plane with a minimum P-wave velocity perpendicular to it (Fig. 15a), as already observed in undeformed sandstone due to preferential pore space elongation (Benson et al., 2005), or could have been slightly triaxial due to the preferred grain alignment parallel to the depositional flow. In the latter case, the P-wave velocity within the bedding plane would have been anisotropic with the two principal in plane values still considerably larger than the one perpendicular to the bedding. Under subhorizontal tectonic loading, the sandstone grains developed intense intragranular cracking in a parallel set of microcracks perpendicular to the bedding strike and aligned with the regional paleo- and contemporaneous stress orientation (Fig. 15b).

A final question that remains unanswered is the genesis of microcracks and anisotropy in the TCDP sandstone. Since the crack planes preferred orientations we infer are subvertical (Fig. 15b), it is unlikely that the microcracking was due to stress relief. With

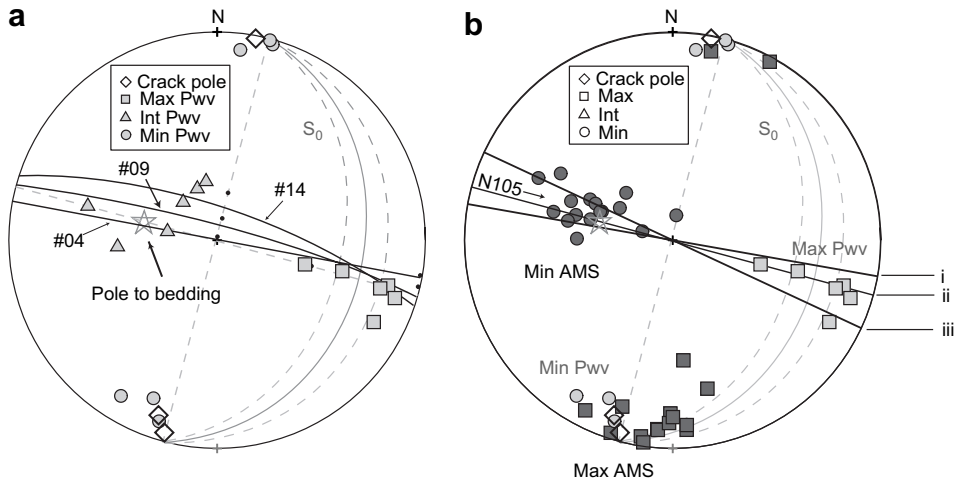

Fig. 14. (a) Planar best fit joining the three intercept minima directions (i.e. preferred crack orientation in each plane) for each plug set of Fig. 13. The normal to the planes obtained for all sets (crack poles) falls in the region of minimum P-wave velocity, parallel to the bedding strike. (b) Comparison of AMS of TCDP samples and APV eigenvectors of sandstones with stress orientation inferred by Angelier et al. (1986), Yeh et al. (2007), Wu et al. (2007) and Lin et al. (2007a). Minimum susceptibility axes are parallel to the average bedding pole measured in the TCDP hole (Yeh et al., 2007). Maximum susceptibility axes are located close to the intersection between the bedding and the plane normal to the paleostress trajectory of Angelier et al. (1986) and to the direction of the maximum horizontal stress S_{Hmax} deduced from borehole breakouts and tensile fractures in holes A (Wu et al., 2007) and B (Lin et al., 2007a). Maximum P-wave velocity axes are subparallel to the paleostress trajectory and to the maximum horizontal stress S_{Hmax}. Minimum P-wave velocity axes are perpendicular to S_{Hmax} and parallel to the bedding strike. (i) N100: Stress trajectory deduced from fold axes (Angelier et al., 1986). (ii) N105: Average bedding dip direction in hole A (Yeh et al., 2007); paleostress trajectory deduced from fault analysis (Angelier et al., 1986). (iii) N115: Average orientation of S_{Hmax} deduced from borehole breakouts and tensile fractures in Hole A (Wu et al., 2007) and B (Lin et al., 2007a).

reference to the current stress state associated with reverse faulting, the average crack normal direction is indeed aligned with the intermediate principal stress. Since fracture mechanics predicts brittle cracking to develop with the normal to cracks parallel to the minimum principal stress, the stress field responsible for inducing microcracking in the sandstone cannot be identical to the stress field associated with the kinematics of the Chelungpu fault. Recent studies on borehole breakouts and tensile fractures (Lin et al., 2007a; Wu et al., 2007) in TCDP holes A and B have identified stress orientation changes likely associated to the 1999 seismic event. Principal stress rotation was also showed by anelastic strain recovery (ASR) experiments (Lin et al., 2007a). In this latter study, the authors inferred the orientation of the three principal stresses in three hole A samples retrieved from the deeper Cholan formation underneath the Sanyi thrust, from FZA1111 in the Chinsui shale and from above the Chelungpu fault zone within the shallow Cholan formation. An interesting observation is the fact that the location of the maximum principal stress was found in both shallow samples (i.e. within and above FZA1111) close to the vertical direction, therefore close to the acting direction of the overburden. Lin et al. (2007a) suggested that the stress rotation observed in hole B at FZB1133 (equivalent of FZA1111; Hirono et al., 2007) was reflecting a present post-earthquake stress state consistent with a normal faulting or strike slip regime. Moreover, Yeh et al. (2007) identified

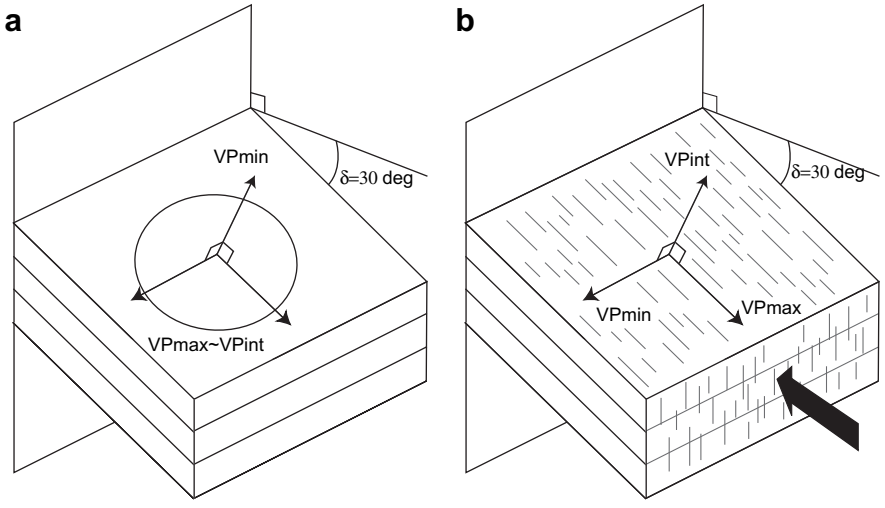

Fig. 15. Explanatory scheme for the P-wave velocities measured in the sandstone samples. (a) The intact rock displays a sedimentary anisotropy with a minimum velocity axis aligned with the bedding pole and the maximum and intermediate axes scattered within the bedding plane. (b) The formation of microcracks lowers the P-wave velocity along the crack normal while elastic moduli remain unchanged in other directions. The result is a rotation of the minimum velocity axis from the bedding pole to the bedding strike and a localization of the maximum velocity axis along the shortening direction, at the intersection between the bedding and cracks planes.

among fault zones numerous strike slip structures dipping ~N15–60/75, sometimes with a normal slip component and in one case (FZA1221) overprinting bedding slip thrusts. These observations are consistent with a transitory minimum principal stress that would be oriented parallel to the bedding strike. In Fig. 13, cracks orientation in *X* samples at depths 1365 m and 1394.25 m (sets #09 and #14) are somewhat offset from the originally inferred vertical direction (maximum at 65–70°), which might be an indication of a genetic relationship with the strike slip faults identified by Yeh et al. (2007). The actual mechanics responsible for this transitory stress state remain uncertain and necessitate more investigations including continuous in situ monitoring of stress changes associated to fault rupturing. Some possible contributors that may be put forth are (1) contrasting elastic properties between siltstone and sandstone layers, (2) post rupturing viscous response generating a transient tensile stress parallel to the bedding strike, or (3) mechanical anisotropy favoring N15 extension under acting overburden.

Our investigations underscored the relatively strong anisotropy of two physical properties in relation to bedding foliation and tectonic loading. This implies that anisotropy in the mechanical and transport properties of the TCDP cores could be significant. Systematic studies of mechanical properties, frictional strength and permeability of TCDP cores are currently underway in a number of laboratories. While our study provides a petrofabric framework, we expect that these ongoing studies will provide useful insight into the mechanics of earthquake rupture in the Chelungpu fault system.

Acknowledgments

The research at Stony Brook was partially supported by the U.S. Geological Survey under grants 05HQGR0065 and 06HQGR0030. The research at Cergy-Pontoise was supported by the CNRS. The research at NTU was supported by the National Science Council of Taiwan under grant NSC 92-2119-M-002-006. We thank Jean-Christian Colombier for helping with the measurements and the two reviewers J.P. Gratier and G.J. Borradaile for their thorough and helpful reviews.

References

Angelier, J., Barrier, E., Chu, H.T., 1986. Plate collision and paleostress trajectories in a fold thrust belt—the foothills of Taiwan. Tectonophysics 125 (1-3), 161–178.

Averbuch, O., Frizon de Lamotte, D., Kissel, C., 1992. Magnetic fabric as a structural indicator of the deformation path within a fold-thrust structure: a test case from the Corbières (NE Pyrenees, France). Journal of Structural Geology 14 (4), 461–474.

Benson, P.M., Meredith, P.G., Platzman, E.S., White, R.E., 2005. Pore fabric shape anisotropy in porous sandstones and its relation to elastic wave velocity and permeability anisotropy under hydrostatic pressure. International Journal of Rock Mechanics and Mining Sciences 42 (7-8), 890–899.

Borradaile, G.J., Henry, B., 1997. Tectonic applications of magnetic susceptibility and its anisotropy. Earth-Science Reviews 42, 49–93.

Borradaile, G.J., Jackson, M., 2004. Anisotropy of magnetic susceptibility (AMS): magnetic petrofabrics of deformed rocks. Geological Society of London Special Publications 238, 299–360.

Borradaile, G.J., Stupavsky, M., 1995. Anisotropy of magnetic susceptibility: measurement schemes. Geophysical Research Letters 22, 1957–1960.

Brückmann, W., Moran, K., Housen, B., 1997. Acoustic anisotropy and microfabric development in accreted sediment from the Nankai trough. Proceedings of the Ocean Drilling Program. Scientific Results 131, 221–233.

Brückmann, W., Moran, K., Taylor, E., 1993. Acoustic anisotropy and microfabric development in accreted sediment from the Nankai trough. Proceedings of the Ocean Drilling Program. Scientific Results 131, 221–233.

Budiansky, B., O'Connell, R.J., 1976. Elastic-moduli of a cracked solid. International Journal of Solids and Structures 12 (2), 81–97.

Byrne, T., Maltman, A., Stephenson, E., Soh, W., Knipe, R., 1993. Deformation structures and fluid flow in the tow region of the Nankai accretionary prism. Proceedings of the Ocean Drilling Program. Scientific Results 131, 83–101.

Daly, L., 1970. Etude des propriétés magnétiques des roches métamorphiques ou simplement tectonisées. Nature de leur aimantation naturelle. Détermination de leur anisotropie magnétique et application à l'analyse structurale, PhD thesis, Université Paris VI.

David, C., Datot, M., Jeannette, D., 1993. Pore structures and transport properties of sandstone. Transport Porous Media 11, 161–177.

Graham, J.W., 1966. Significance of magnetic anisotropy in appalachian sedimentary rocks. In: Steinhart, J.S., Smith, T.J. (Eds.), The Earth Beneath the ContinentsAmerican Geophysical Union Geophysical Monograph Series 10, pp. 627–648.

Hirono, T., Yeh, E.-C., Lin, W., Sone, H., Mishima, T., Soh, W., Hashimoto, Y., Matsubayashi, O., Aoike, K., Ito, H., Kinoshita, M., Murayama, M., Song, S.-R., Ma, K.-F., Hung, J.-H., Wang, C.-Y., Tsai, Y.-B., Kondo, T., Nishimura, M., Moriya, S., Tanaka, T., Fujiki, T., Maeda, L., Muraki, H., Kuramoto, T., Sugiyama, K., Sugarawa, T., 2007. Nondestructive continuous physical property measurements of core samples recovered from Hole B, Taiwan Chelungpu-Fault Drilling Project. Journal of Geophysical Research 112 B07404.

Hornby, B.E., 1998. Experimental laboratory determination of the dynamic elastic properties of wet, drained shales. Journal of Geophysical Research-Solid Earth 103 (B12), 29945–29964.

Housen, B.A., 1997. Magnetic anisotropy of Barbados prism sediments. Proceedings of the Ocean Drilling Program. Scientific Results 156, 97–105.

Hrouda, F., Zdenek, P., Wohlgemuth, J., 1993. Development of magnetic and elastic anisotropies in slates during progressive deformation. Physics of the Earth and Planetary Interiors 77, 251–265.

Isaacs, A.J., Evans, J.P., Song, S.-R., Kolesar, P.T., 2007. Structural, mineralogical, and geochemical characterization of the Chelungpu thrust fault, Taiwan. Terrestrial. Atmospheric and Oceanic Sciences 18 (2), 183–221.

Jelinek, V., 1981. Characterization of the magnetic fabrics of rocks. Tectonophysics 79, T63–T67.

Johnston, J.E., Christensen, N.I., 1995. Seismic anisotropy of shales. Journal of Geophysical Research 100 (B4), 5991–6003.

Kano, Y., Mori, J., Fujio, R., Ito, H., Yanagidani, T., Nakao, S., Ma, K.F., 2006. Heat signature on the Chelungpu fault associated with the 1999 Chi-Chi, Taiwan earthquake. Geophysical Research Letters 33 (14).

Kern, H., 1993. P- and S-wave anisotropy and shear-wave splitting at pressure and temperature in possible mantle rocks and their relation to the rock fabric. Physics of the Earth and Planetary Interiors 78 (3-4), 245–256.

Kligfield, R., Owens, W.H., Lowrie, W., 1981. Magnetic-susceptibility anisotropy, strain, and progressive deformation in Permian sediments from the Maritime Alps (France). Earth and Planetary Science Letters 55 (1), 181–189.

Kuo, L.W.S., Song, S.R., 2005. Characteristics of clay mineralogy in the fault zone of the TCDP and its implication. Abstract of the Annual Meeting of the Geological Society located in Taipei, 45.

Lin, W.R., Yeh, E.-C., Ito, H., Hirono, T., Soh, W., Wang, C.-Y., Ma, K.-F., Hung, J.-H., Song, S.-R., 2007a. Preliminary results of stress measurement using drill cores of TCDP Hole-A: an application of anelastic strain recovery method to three-dimensional in-situ stress determination. Terrestrial. Atmospheric and Oceanic Sciences 18 (2), 379–393.

Lin, W.R., Yeh, E.-C., Ito, H., Hirono, T., Soh, W., Ma, K.-F., Kinoshita, M.W., Wang, C.-Y., Hung, J.-H., Song, S.-R., 2007b. Current stress state and principal stress rotations in the vicinity of the Chelungpu fault induced by the 1999 Chi-Chi, Taiwan, earthquake. Geophysical Research Letters 34, L16307.

Lo, T.-W., Coyner, K.B., Toksöz, M.N., 1986. Experimental determination of elastic anisotropy of Berea Sandstone, Chicopee shale, and Chelmsford granite. Geophysics 51, 164–171.

Louis, L., David, C., Metz, V., Robion, P., Menendez, B., Kissel, C., 2005. Microstructural control on the anisotropy of elastic and transport properties in undeformed sandstones. International Journal of Rock Mechanics 42 (7-8), 911–923.

Louis, L., David, C., Robion, P., 2003. Comparison of the anisotropic behaviour of undeformed sandstones under dry and saturated conditions. Tectonophysics 370 (1-4), 193–212.

Louis, L., Robion, P., David, C., 2004. A single method for the inversion of anisotropic data sets with application to structural studies. Journal of Structural Geology 26, 2065–2072.

Martin-Hernandez, F., Hirt, A.M., 2003. The anisotropy of magnetic susceptibility in biotite, muscovite and chlorite single crystals. Tectonophysics 367, 13–28.

Nur, A., Simmons, G., 1969. The effect of saturation on velocity in low porosity rocks. Earth and Planetary Science Letters 7, 183–193.

Nye, J.F., 1957. Physical Properties of Crystals: Their Representation by Tensors and Matrices. Oxford Science Publications.

Owens, W.H., 1993. Magnetic fabric studies of samples from Hole 808C, Nankai Trough. Proceedings of the Ocean Drilling Program. Scientific Results 131, 301–310.

Pares, J.M., van der Pluijm, B.A., 2002. Evaluating magnetic lineations (AMS) in deformed rocks. Tectonophysics 350 (4), 283–298.

Pfleiderer, S., Halls, H.C., 1993. Magnetic fabric analysis: verification through autocorrelation. Journal of Geophysical Research 98, 4311–4316.

Pokorny, J., Suza, P., Hrouda, F., 2004. Anisotropy of magnetic susceptibility of rocks measured in variable weak magnetic fields using the KLY-4S Kappabridge. Geological Society of London Special Publications 238 (1), 69–76.

Robion, P., Grelaud, S., de Lamotte, D.F., 2007. Pre-folding magnetic fabrics in fold-and-thrust belts: Why the apparent internal deformation of the sedimentary rocks from the Minervois basin (NE-Pyrenees, France) is so high compared to the Potwar basin (SW-Himalaya, Pakistan)? Sedimentary Geology 196 (1-4), 181–200.

Rochette, P., Jackson, M.J., Aubourg, C., 1992. Rock magnetism and the interpretation of anisotropy of magnetic susceptibility. Reviews of Geophysics 30, 209–226.

Sans, M., Verges, J., Gomis, E., Pares, J.M., Schiattarella, M., Trave, A., Calvet, F., Santanach, P., Doulcet, A., 2003. Layer parallel shortening in salt-detached folds: constraint on cross-section restoration. Tectonophysics 372, 85–103.

Shin, T.C., Teng, T.L., 2001. An overview of the 1999 Chi-Chi, Taiwan, earthquake. Bulletin of the Seismological Society of America 91 (5), 895–913.

Song, S.R., Wang, C.Y., Hung, J.H., Ma, K.F., 2007a. Preface to the special issue on Taiwan Chelungpu-fault Drilling Project (TCDP): Site characteristics and on-site measurements. Terrestrial Atmospheric and Oceanic Sciences 18 (2), I–V.

Song, S.R., Kuo, L.W., Yeh, E.C., Wang, C.Y., Hung, J.H., Ma, K.F., 2007b. Characteristics of the lithology, fault-related rocks and fault zone structures in TCDP Hole-A. Terrestrial Atmospheric and Oceanic Sciences 18 (2), 243–269.

Tarling, D.H., Hrouda, F., 1993. The Magnetic Anisotropy of Rocks. Chapman and Hall, London.

Thomsen, L., 1986. Weak elastic anisotropy. Geophysics 51 (10), 1954–1966.

Tsvankin, I., 1997. Anisotropic parameters and P-wave velocity for orthorhombic media. Geophysics 62 (4), 1292–1309.

Underwood, E.E., 1970. Quantitative Stereology. Addison-Wesley, Boston, MA.

Wu, H.Y., Ma, K.F., Zoback, M., Boness, N., Ito, H., Hung, J.H., Hickman, S., 2007. Stress orientations of Taiwan Chelungpu-Fault Drilling Project (TCDP) hole-A as observed from geophysical logs. Geophysical Research Letters 34 (1).

Wu, X.Y., Baud, P., Wong, T.F., 2000. Micromechanics of compressive failure and spatial evolution of anisotropic damage in Darley Dale sandstone. International Journal of Rock Mechanics and Mining Sciences 37 (1-2), 143–160.

Yeh, E., Sone, H., Nakaya, T., Ian, K., Song, S., Hung, J., 2004. Preliminary summary of current fault zones in the Hole-A of TCDP. Eos Transactions AGU, Fall Meeting, Supplement 85 (47).

Yeh, E.C., Sone, H., Nakaya, T., Ian, K.-H., Song, S.-R., Hung, J.-H., Lin, W., Hirono, T., Wang, C.-Y., Ma, K.-F., Soh, W., Kinoshita, M., 2007. Core description and characteristics of fault zones from Hole-A of the Taiwan Chelungpu-Fault drilling project. Terrestrial, Atmospheric and Oceanic Sciences 18 (2), 327–357.

Yue, L.F., Suppe, J., Hung, J.H., 2005. Structural geology of a classic thrust belt earthquake: the 1999 Chi-Chi earthquake Taiwan (M-w=7.6). Journal of Structural Geology 27 (11), 2058–2083.